Polarization and Entanglement in Baryon-Antibaryon Pair Production in Electron-Positron Annihilation

M. Ablikim[1], M. N. Achasov[10,d], S. Ahmed[15], M. Albrecht[4], M. Alekseev[55A,55C], A. Amoroso[55A,55C], F. F. An[1], Q. An[52,42], Y. Bai[41], O. Bakina[27], R. Baldini Ferroli[23A], Y. Ban[35], K. Begzsuren[25], D. W. Bennett[22], J. V. Bennett[5], N. Berger[26], M. Bertani[23A], D. Bettoni[24A], F. Bianchi[55A,55C], E. Boger[27,b], I. Boyko[27], R. A. Briere[5], H. Cai[57], X. Cai[1,42], A. Calcaterra[23A], G. F. Cao[1,46], S. A. Cetin[45B], J. Chai[55C], J. F. Chang[1,42], W. L. Chang[1,46], G. Chelkov[27,b,c], G. Chen[1], H. S. Chen[1,46], J. C. Chen[1], M. L. Chen[1,42], P. L. Chen[53], S. J. Chen[33], X. R. Chen[30], Y. B. Chen[1,42], W. Cheng[55C], X. K. Chu[35], G. Cibinetto[24A], F. Cossio[55C], H. L. Dai[1,42], J. P. Dai[37,h], A. Dbeyssi[15], D. Dedovich[27], Z. Y. Deng[1], A. Denig[26], I. Denysenko[27], M. Destefanis[55A,55C], F. De Mori[55A,55C], Y. Ding[31], C. Dong[34], J. Dong[1,42], L. Y. Dong[1,46], M. Y. Dong[1,42,46], Z. L. Dou[33], S. X. Du[60], P. F. Duan[1], J. Z. Fan[44], J. Fang[1,42], S. S. Fang[1,46], Y. Fang[1], R. Farinelli[24A,24B], L. Fava[55B,55C], S. Fegan[26], F. Feldbauer[4], G. Felici[23A], C. Q. Feng[52,42], E. Fioravanti[24A], M. Fritsch[4], C. D. Fu[1], Q. Gao[1], X. L. Gao[52,42], Y. Gao[44], Y. G. Gao[6], Z. Gao[52,42], B. Garillon[26], I. Garzia[24A], A. Gilman[49], K. Goetzen[11], L. Gong[34], W. X. Gong[1,42], W. Gradl[26], M. Greco[55A,55C], L. M. Gu[33], M. H. Gu[1,42], Y. T. Gu[13], A. Q. Guo[1], L. B. Guo[32], R. P. Guo[1,46], Y. P. Guo[26], A. Guskov[27], Z. Haddadi[29], S. Han[57], X. Q. Hao[16], F. A. Harris[47], K. L. He[1,46], F. H. Heinsius[4], T. Held[4], Y. K. Heng[1,42,46], Z. L. Hou[1], H. M. Hu[1,46], J. F. Hu[37,h], T. Hu[1,42,46], Y. Hu[1], G. S. Huang[52,42], J. S. Huang[16], X. T. Huang[36], X. Z. Huang[33], Z. L. Huang[31], T. Hussain[54], W. Ikegami Andersson[56], M. Irshad[52,42], Q. Ji[1], Q. P. Ji[16], X. B. Ji[1,46], X. L. Ji[1,42], H. L. Jiang[36], X. S. Jiang[1,42,46], X. Y. Jiang[34], J. B. Jiao[36], Z. Jiao[18], D. P. Jin[1,42,46], S. Jin[33], Y. Jin[48], T. Johansson[56], A. Julin[49], N. Kalantar-Nayestanaki[29], X. S. Kang[34], M. Kavatsyuk[29], B. C. Ke[1], I. K. Keshk[4], T. Khan[52,42], A. Khoukaz[50], P. Kiese[26], R. Kiuchi[1], R. Kliemt[11], L. Koch[28], O. B. Kolcu[45B,f], B. Kopf[4], M. Kornicer[47], M. Kuemmel[4], M. Kuessner[4], A. Kupsc[56], M. Kurth[1], W. Kühn[28], J. S. Lange[28], P. Larin[15], L. Lavezzi[55C], S. Leiber[4], H. Leithoff[26], C. Li[56], Cheng Li[52,42], D. M. Li[60], F. Li[1,42], F. Y. Li[35], G. Li[1], H. B. Li[1,46], H. J. Li[1,46], J. C. Li[1], J. W. Li[40], K. J. Li[43], Kang Li[14], Ke Li[1], Lei Li[3], P. L. Li[52,42], P. R. Li[46,7], Q. Y. Li[36], T. Li[36], W. D. Li[1,46], W. G. Li[1], X. L. Li[36], X. N. Li[1,42], X. Q. Li[34], Z. B. Li[43], H. Liang[52,42], Y. F. Liang[39], Y. T. Liang[28], G. R. Liao[12], L. Z. Liao[1,46], J. Libby[21], C. X. Lin[43], D. X. Lin[15], B. Liu[37,h], B. J. Liu[1], C. X. Liu[1], D. Liu[52,42], D. Y. Liu[37,h], F. H. Liu[38], Fang Liu[1], Feng Liu[6], H. B. Liu[13], H. L Liu[41], H. M. Liu[1,46], Huanhuan Liu[1], Huihui Liu[17], J. J. Liu[1], J. B. Liu[52,42], J. Y. Liu[1,46], K. Y. Liu[31], Ke Liu[6], L. D. Liu[35], Q. Liu[46], S. B. Liu[52,42], X. Liu[30], Y. B. Liu[34], Z. A. Liu[1,42,46], Zhiqing Liu[26], Y. F. Long[35], X. C. Lou[1,42,46], H. J. Lu[18], J. G. Lu[1,42], Y. Lu[1], Y. P. Lu[1,42], C. L. Luo[32], M. X. Luo[59], P. W. Luo[43], T. Luo[9,j], X. L. Luo[1,42], S. Lusso[55C], X. R. Lyu[46], F. C. Ma[31], H. L. Ma[1], L. L. Ma[36], M. M. Ma[1,46], Q. M. Ma[1], X. N. Ma[34], X. Y. Ma[1,42], Y. M. Ma[36], F. E. Maas[15], M. Maggiora[55A,55C], S. Maldaner[26], Q. A. Malik[54], A. Mangoni[23B], Y. J. Mao[35], Z. P. Mao[1], S. Marcello[55A,55C], Z. X. Meng[48], J. G. Messchendorp[29], G. Mezzadri[24A], J. Min[1,42], T. J. Min[33], R. E. Mitchell[22], X. H. Mo[1,42,46], Y. J. Mo[6], C. Morales Morales[15], N. Yu. Muchnoi[10,d], H. Muramatsu[49], A. Mustafa[4], S. Nakhoul[11,g], Y. Nefedov[27], F. Nerling[11,g], I. B. Nikolaev[10,d], Z. Ning[1,42], S. Nisar[8], S. L. Niu[1,42], X. Y. Niu[1,46], S. L. Olsen[46], Q. Ouyang[1,42,46], S. Pacetti[23B], Y. Pan[52,42], M. Papenbrock[56], P. Patteri[23A], M. Pelizaeus[4], J. Pellegrino[55A,55C], H. P. Peng[52,42], Z. Y. Peng[13], K. Peters[11,g], J. Pettersson[56], J. L. Ping[32], R. G. Ping[1,46], A. Pitka[4], R. Poling[49], V. Prasad[52,42], H. R. Qi[2], M. Qi[33], T. Y. Qi[2], S. Qian[1,42], C. F. Qiao[46], N. Qin[57], X. S. Qin[4], Z. H. Qin[1,42], J. F. Qiu[1], S. Q. Qu[34], K. H. Rashid[54,i], C. F. Redmer[26], M. Richter[4], M. Ripka[26], A. Rivetti[55C], M. Rolo[55C], G. Rong[1,46], Ch. Rosner[15], M. Rump[50], A. Sarantsev[27,e], M. Savrié[24B], K. Schoenning[56], W. Shan[19], X. Y. Shan[52,42], M. Shao[52,42], C. P. Shen[2], P. X. Shen[34], X. Y. Shen[1,46], H. Y. Sheng[1], X. Shi[1,42], J. J. Song[36], W. M. Song[36], X. Y. Song[1], S. Sosio[55A,55C], C. Sowa[4], S. Spataro[55A,55C], F. F. Sui[36], G. X. Sun[1], J. F. Sun[16], L. Sun[57], S. S. Sun[1,46], X. H. Sun[1], Y. J. Sun[52,42], Y. K Sun[52,42], Y. Z. Sun[1], Z. J. Sun[1,42], Z. T. Sun[1], Y. T Tan[52,42], C. J. Tang[39], G. Y. Tang[1], X. Tang[1], M. Tiemens[29], B. Tsednee[25], I. Uman[45D], B. Wang[1], B. L. Wang[46], C. W. Wang[33], D. Wang[35], D. Y. Wang[35], Dan Wang[46], H. H. Wang[36], K. Wang[1,42], L. L. Wang[1], L. S. Wang[1], M. Wang[36], Meng Wang[1,46], P. Wang[1], P. L. Wang[1], W. P. Wang[52,42], X. F. Wang[1], Y. Wang[52,42], Y. F. Wang[1,42,46], Z. Wang[1,42], Z. G. Wang[1,42], Z. Y. Wang[1], Zongyuan Wang[1,46], T. Weber[4], D. H. Wei[12], P. Weidenkaff[26], S. P. Wen[1], U. Wiedner[4], M. Wolke[56], L. H. Wu[1], L. J. Wu[1,46], Z. Wu[1,42], L. Xia[52,42], X. Xia[36], Y. Xia[20], D. Xiao[1], Y. J. Xiao[1,46], Z. J. Xiao[32], Y. G. Xie[1,42], Y. H. Xie[6], X. A. Xiong[1,46], Q. L. Xiu[1,42], G. F. Xu[1], J. J. Xu[1,46], L. Xu[1], Q. J. Xu[14], X. P. Xu[40], F. Yan[53], L. Yan[55A,55C], W. B. Yan[52,42], W. C. Yan[2], Y. H. Yan[20], H. J. Yang[37,h], H. X. Yang[1], L. Yang[57], R. X. Yang[52,42], S. L. Yang[1,46], Y. H. Yang[33], Y. X. Yang[12], Yifan Yang[1,46], Z. Q. Yang[20], M. Ye[1,42], M. H. Ye[7], J. H. Yin[1], Z. Y. You[43], B. X. Yu[1,42,46], C. X. Yu[34], J. S. Yu[20], C. Z. Yuan[1,46], Y. Yuan[1], A. Yuncu[45B,a], A. A. Zafar[54], Y. Zeng[20], B. X. Zhang[1], B. Y. Zhang[1,42], C. C. Zhang[1], D. H. Zhang[1], H. H. Zhang[43], H. Y. Zhang[1,42], J. Zhang[1,46], J. L. Zhang[58], J. Q. Zhang[4], J. W. Zhang[1,42,46], J. Y. Zhang[1], J. Z. Zhang[1,46], K. Zhang[1,46], L. Zhang[44], S. F. Zhang[33], T. J. Zhang[37,h], X. Y. Zhang[36], Y. Zhang[52,42], Y. H. Zhang[1,42],

Y. T. Zhang[52,42], Yang Zhang[1], Yao Zhang[1], Yu Zhang[46], Z. H. Zhang[6], Z. P. Zhang[52], Z. Y. Zhang[57], G. Zhao[1], J. W. Zhao[1,42], J. Y. Zhao[1,46], J. Z. Zhao[1,42], Lei Zhao[52,42], Ling Zhao[1], M. G. Zhao[34], Q. Zhao[1], S. J. Zhao[60], T. C. Zhao[1], Y. B. Zhao[1,42], Z. G. Zhao[52,42], A. Zhemchugov[27,b], B. Zheng[53], J. P. Zheng[1,42], W. J. Zheng[36], Y. H. Zheng[46], B. Zhong[32], L. Zhou[1,42], Q. Zhou[1,46], X. Zhou[57], X. K. Zhou[52,42], X. R. Zhou[52,42], X. Y. Zhou[1], Xiaoyu Zhou[20], Xu Zhou[20], A. N. Zhu[1,46], J. Zhu[34], J. Zhu[43], K. Zhu[1], K. J. Zhu[1,42,46], S. Zhu[1], S. H. Zhu[51], X. L. Zhu[44], Y. C. Zhu[52,42], Y. S. Zhu[1,46], Z. A. Zhu[1,46], J. Zhuang[1,42], B. S. Zou[1], J. H. Zou[1]

(BESIII Collaboration)

[1] *Institute of High Energy Physics, Beijing 100049, People's Republic of China*
[2] *Beihang University, Beijing 100191, People's Republic of China*
[3] *Beijing Institute of Petrochemical Technology, Beijing 102617, People's Republic of China*
[4] *Bochum Ruhr-University, D-44780 Bochum, Germany*
[5] *Carnegie Mellon University, Pittsburgh, Pennsylvania 15213, USA*
[6] *Central China Normal University, Wuhan 430079, People's Republic of China*
[7] *China Center of Advanced Science and Technology, Beijing 100190, People's Republic of China*
[8] *COMSATS Institute of Information Technology, Lahore, Defence Road, Off Raiwind Road, 54000 Lahore, Pakistan*
[9] *Fudan University, Shanghai 200443, People's Republic of China*
[10] *G.I. Budker Institute of Nuclear Physics SB RAS (BINP), Novosibirsk 630090, Russia*
[11] *GSI Helmholtzcentre for Heavy Ion Research GmbH, D-64291 Darmstadt, Germany*
[12] *Guangxi Normal University, Guilin 541004, People's Republic of China*
[13] *Guangxi University, Nanning 530004, People's Republic of China*
[14] *Hangzhou Normal University, Hangzhou 310036, People's Republic of China*
[15] *Helmholtz Institute Mainz, Johann-Joachim-Becher-Weg 45, D-55099 Mainz, Germany*
[16] *Henan Normal University, Xinxiang 453007, People's Republic of China*
[17] *Henan University of Science and Technology, Luoyang 471003, People's Republic of China*
[18] *Huangshan College, Huangshan 245000, People's Republic of China*
[19] *Hunan Normal University, Changsha 410081, People's Republic of China*
[20] *Hunan University, Changsha 410082, People's Republic of China*
[21] *Indian Institute of Technology Madras, Chennai 600036, India*
[22] *Indiana University, Bloomington, Indiana 47405, USA*
[23] *(A)INFN Laboratori Nazionali di Frascati, I-00044, Frascati, Italy; (B)INFN and University of Perugia, I-06100, Perugia, Italy*
[24] *(A)INFN Sezione di Ferrara, I-44122, Ferrara, Italy; (B)University of Ferrara, I-44122, Ferrara, Italy*
[25] *Institute of Physics and Technology, Peace Ave. 54B, Ulaanbaatar 13330, Mongolia*
[26] *Johannes Gutenberg University of Mainz, Johann-Joachim-Becher-Weg 45, D-55099 Mainz, Germany*
[27] *Joint Institute for Nuclear Research, 141980 Dubna, Moscow region, Russia*
[28] *Justus-Liebig-Universitaet Giessen, II. Physikalisches Institut, Heinrich-Buff-Ring 16, D-35392 Giessen, Germany*
[29] *KVI-CART, University of Groningen, NL-9747 AA Groningen, The Netherlands*
[30] *Lanzhou University, Lanzhou 730000, People's Republic of China*
[31] *Liaoning University, Shenyang 110036, People's Republic of China*
[32] *Nanjing Normal University, Nanjing 210023, People's Republic of China*
[33] *Nanjing University, Nanjing 210093, People's Republic of China*
[34] *Nankai University, Tianjin 300071, People's Republic of China*
[35] *Peking University, Beijing 100871, People's Republic of China*
[36] *Shandong University, Jinan 250100, People's Republic of China*
[37] *Shanghai Jiao Tong University, Shanghai 200240, People's Republic of China*
[38] *Shanxi University, Taiyuan 030006, People's Republic of China*
[39] *Sichuan University, Chengdu 610064, People's Republic of China*
[40] *Soochow University, Suzhou 215006, People's Republic of China*
[41] *Southeast University, Nanjing 211100, People's Republic of China*
[42] *State Key Laboratory of Particle Detection and Electronics, Beijing 100049, Hefei 230026, People's Republic of China*
[43] *Sun Yat-Sen University, Guangzhou 510275, People's Republic of China*
[44] *Tsinghua University, Beijing 100084, People's Republic of China*
[45] *(A)Ankara University, 06100 Tandogan, Ankara, Turkey; (B)Istanbul Bilgi University, 34060 Eyup, Istanbul, Turkey; (C)Uludag University, 16059 Bursa, Turkey; (D)Near East University, Nicosia, North Cyprus, Mersin 10,*

Turkey
[46] *University of Chinese Academy of Sciences, Beijing 100049, People's Republic of China*
[47] *University of Hawaii, Honolulu, Hawaii 96822, USA*
[48] *University of Jinan, Jinan 250022, People's Republic of China*
[49] *University of Minnesota, Minneapolis, Minnesota 55455, USA*
[50] *University of Muenster, Wilhelm-Klemm-Str. 9, 48149 Muenster, Germany*
[51] *University of Science and Technology Liaoning, Anshan 114051, People's Republic of China*
[52] *University of Science and Technology of China, Hefei 230026, People's Republic of China*
[53] *University of South China, Hengyang 421001, People's Republic of China*
[54] *University of the Punjab, Lahore-54590, Pakistan*
[55] *(A)University of Turin, I-10125, Turin, Italy; (B)University of Eastern Piedmont, I-15121, Alessandria, Italy; (C)INFN, I-10125, Turin, Italy*
[56] *Uppsala University, Box 516, SE-75120 Uppsala, Sweden*
[57] *Wuhan University, Wuhan 430072, People's Republic of China*
[58] *Xinyang Normal University, Xinyang 464000, People's Republic of China*
[59] *Zhejiang University, Hangzhou 310027, People's Republic of China*
[60] *Zhengzhou University, Zhengzhou 450001, People's Republic of China*

[a] *Also at Bogazici University, 34342 Istanbul, Turkey*
[b] *Also at the Moscow Institute of Physics and Technology, Moscow 141700, Russia*
[c] *Also at the Functional Electronics Laboratory, Tomsk State University, Tomsk, 634050, Russia*
[d] *Also at the Novosibirsk State University, Novosibirsk, 630090, Russia*
[e] *Also at the NRC "Kurchatov Institute", PNPI, 188300, Gatchina, Russia*
[f] *Also at Istanbul Arel University, 34295 Istanbul, Turkey*
[g] *Also at Goethe University Frankfurt, 60323 Frankfurt am Main, Germany*
[h] *Also at Key Laboratory for Particle Physics, Astrophysics and Cosmology, Ministry of Education; Shanghai Key Laboratory for Particle Physics and Cosmology; Institute of Nuclear and Particle Physics, Shanghai 200240, People's Republic of China*
[i] *Also at Government College Women University, Sialkot - 51310. Punjab, Pakistan.*
[j] *Also at Key Laboratory of Nuclear Physics and Ion-beam Application (MOE) and Institute of Modern Physics, Fudan University, Shanghai 200443, People's Republic of China*

(Dated: August 28, 2018)

Using a sample of 1.31×10^9 J/ψ events collected with the BESIII detector, we report the first observation of spin polarization of Λ and $\bar{\Lambda}$ hyperons from the coherent production in the $J/\psi \to \Lambda\bar{\Lambda}$ decay. We measure the phase between the hadronic form factors to be $\Delta\Phi = (42.4 \pm 0.6 \pm 0.5)^\circ$. The decay parameters for $\Lambda \to p\pi^-$ (α_-), $\bar{\Lambda} \to \bar{p}\pi^+$ (α_+) and $\bar{\Lambda} \to \bar{n}\pi^0$ ($\bar{\alpha}_0$) are measured to be $\alpha_- = 0.750 \pm 0.009 \pm 0.004$, $\alpha_+ = -0.758 \pm 0.010 \pm 0.007$ and $\bar{\alpha}_0 = -0.692 \pm 0.016 \pm 0.006$, respectively. The obtained value of α_- is higher by $(17 \pm 3)\%$ than the current world average. In addition, the CP asymmetry $A_{CP} = (\alpha_- + \alpha_+)/(\alpha_- - \alpha_+)$ of $-0.006 \pm 0.012 \pm 0.007$ is extracted with substantially improved precision. The ratio $\bar{\alpha}_0/\alpha_+ = 0.913 \pm 0.028 \pm 0.012$ is also measured.

PACS numbers: 11.80.Cr, 13.20.Gd, 14.20.Jn

I. INTRODUCTION

The well-defined and simple initial state makes baryon-antibaryon pair production at an electron-positron collider an ideal system to test fundamental symmetries in the baryon sector, in particular when the probability of the process is enhanced by a resonance such as the J/ψ [1]. The spin orientations of the baryon and antibaryon are entangled and, for spin one-half baryons, the pair is produced either with the same or opposite helicities. The transition amplitudes to the respective spin states can acquire a relative phase due to the strong interaction in the final state, leading to a time-reversal-odd observable: a transverse spin polarization of the baryons [2, 3]. This effect has previously been neglected for the baryon pairs from J/ψ decays [4], and there is no prediction for this polarization.

Here, we observe baryon polarization for the first time in an electron-positron reaction. The baryon

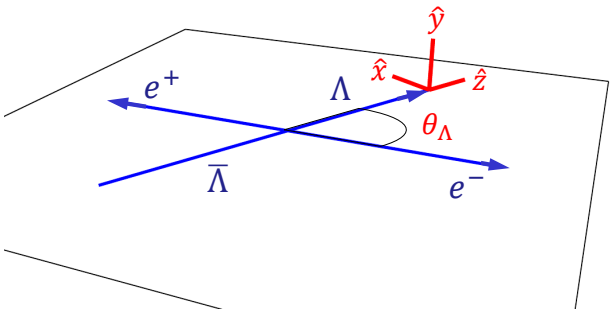

FIG. 1. Kinematics of the reaction $e^+e^- \to J/\psi \to \Lambda\bar{\Lambda}$ in the overall center-of-mass system. The Λ particle is emitted in the $\hat{z}$ direction at an angle θ_Λ with respect to the e^- direction, and the $\bar{\Lambda}$ is emitted in the opposite direction. The hyperons are polarized in the direction perpendicular to the reaction plane ($\hat{y}$). The hyperons are reconstructed, and the polarization is determined by measuring their decay products: (anti-)nucleons and pions.

studied is the Λ hyperon, which decays via a parity non-conserving weak process. The Lambda polarisation is extracted from the angular distribution of its decay products; from this, the production phase is determined to be $(42.4 \pm 0.6 \pm 0.5)^\circ$. The observed polarization allows the simultaneous determination of the Λ and $\bar{\Lambda}$ decay asymmetries from the events, in which all decay products are measured. A sensitive CP symmetry test in the strange baryon sector is performed by directly comparing the asymmetry parameters for $\Lambda \to p\pi^-$ and $\bar{\Lambda} \to \bar{p}\pi^+$.

Of major importance is our result for the $\Lambda \to p\pi^-$ asymmetry parameter. Nearly all experiments making use of the Λ polarization (some examples are given in Refs. [5–12]) use this decay for reconstruction and the $\Lambda \to p\pi^-$ asymmetry parameter in the determination of the polarization. To determine the polarization from the product of the polarization and the asymmetry parameter, all these studies assume an asymmetry parameter of 0.642 ± 0.013, the world-average value established from results spanning 1963–75 [13–17].

The principle of the measurement is illustrated in Fig. 1. In the collision of an electron and positron, a J/ψ resonance is produced at rest in a single photon annihilation process, and it subsequently decays into a $\Lambda\bar{\Lambda}$ pair: $e^+e^- \to J/\psi \to \Lambda\bar{\Lambda}$. The transition between the initial electron-positron pair and the final baryon-antibaryon pair includes helicity conserving and -flip amplitudes [18–22]. Since the electron mass is negligible in comparison to the J/ψ mass, the initial electron and positron helicities have to be opposite. This implies that the angular distribution and polarization of the produced Λ and $\bar{\Lambda}$ particles can be described uniquely by only two real parameters: α_ψ — the $J/\psi \to \Lambda\bar{\Lambda}$ angular distribution parameter, and $\Delta\Phi$ — the phase between the two helicity amplitudes. The value of the parameter α_ψ is well known [23–25], but the phase $\Delta\Phi$ has never been considered before. If $\Delta\Phi \neq 0$, the Λ and $\bar{\Lambda}$ will be polarized in the direction perpendicular to the production plane. The magnitude of the polarization depends on the angle (θ_Λ) between the Λ and the electron beam direction in the J/ψ rest frame (see Fig. 1).

The polarization of the weakly decaying particles, such as the Λ hyperons, can be determined using the angular distribution of the daughter particles. For example, for the $\Lambda \to p\pi^-$ decay, the Λ hyperon polarization vector, $\mathbf{P}_\Lambda$, is given by the angular distribution of the daughter protons via $\frac{1}{4\pi}(1 + \alpha_- \mathbf{P}_\Lambda \cdot \hat{\mathbf{n}})$, where $\hat{\mathbf{n}}$ is the unit vector along the proton momentum in the Λ rest frame and α_- is the asymmetry parameter of the decay [26]. The corresponding parameters α_+ for $\bar{\Lambda} \to \bar{p}\pi^+$, α_0 for $\Lambda \to n\pi^0$, and $\bar{\alpha}_0$ for $\bar{\Lambda} \to \bar{n}\pi^0$ are defined in the same way [27]. The joint angular distribution of $J/\psi \to \Lambda\bar{\Lambda}$ ($\Lambda \to f$ and $\bar{\Lambda} \to \bar{f}$, $f = p\pi^-$ or $n\pi^0$) depends on the Λ and $\bar{\Lambda}$ polarization and spin correlation of the $\Lambda\bar{\Lambda}$ pair via the α_ψ and $\Delta\Phi$ parameters. In particular, the joint angular distribution of the decay chain $J/\psi \to (\Lambda \to p\pi^-)(\bar{\Lambda} \to \bar{p}\pi^+)$ can be expressed as [4]:

$$
\begin{aligned}
\mathcal{W}(\boldsymbol{\xi}; \alpha_\psi, \Delta\Phi, \alpha_-, \alpha_+) =& 1 + \alpha_\psi \cos^2\theta_\Lambda \\
&+ \alpha_-\alpha_+ \left[\sin^2\theta_\Lambda \left(n_{1,x}n_{2,x} - \alpha_\psi n_{1,y}n_{2,y}\right) + \left(\cos^2\theta_\Lambda + \alpha_\psi\right) n_{1,z}n_{2,z}\right] \\
&+ \alpha_-\alpha_+ \sqrt{1-\alpha_\psi{}^2}\cos(\Delta\Phi)\sin\theta_\Lambda\cos\theta_\Lambda \left(n_{1,x}n_{2,z} + n_{1,z}n_{2,x}\right) \\
&+ \sqrt{1-\alpha_\psi{}^2}\sin(\Delta\Phi)\ \sin\theta_\Lambda\cos\theta_\Lambda \left(\alpha_- n_{1,y} + \alpha_+ n_{2,y}\right),
\end{aligned}
\tag{1}
$$

where $\hat{\mathbf{n}}_1$ ($\hat{\mathbf{n}}_2$) is the unit vector in the direction of the nucleon (antinucleon) in the rest frame of Λ ($\bar{\Lambda}$). The components of these vectors are expressed using a common $(\hat{x}, \hat{y}, \hat{z})$ coordinate system with the orientation shown in Fig. 1. The $\hat{z}$ axis in the Λ and $\bar{\Lambda}$ rest frames is oriented along the Λ momentum $\mathbf{p}_\Lambda$ in the J/ψ rest system. The $\hat{y}$ axis is perpendicular to the reaction plane and oriented along the vector $\mathbf{k}_- \times \mathbf{p}_\Lambda$, where $\mathbf{k}_-$ is the electron beam momentum in the J/ψ rest system. The variable $\boldsymbol{\xi}$ denotes the tuple $(\theta_\Lambda, \hat{\mathbf{n}}_1, \hat{\mathbf{n}}_2)$, a set of kinematic variables which uniquely specify an event configuration. The terms multiplied by $\alpha_-\alpha_+$ in Eq. (1) represent the contribution from $\Lambda\bar{\Lambda}$ spin correlations, while the terms multiplied by α_- and α_+ separately represent the contribution from the polarization. The presence of all three contributions in Eq. (1) enables an unambiguous determination of the parameters α_ψ and $\Delta\Phi$ and the decay asymmetries α_-, α_+. If $\bar{\Lambda}$ is reconstructed via its $\bar{n}\pi^0$ decay, the parameters α_ψ, $\Delta\Phi$ and the decay asymmetries α_- and $\bar{\alpha}_0$ can be determined independently, since the corresponding angular distribution is obtained by replacing α_+ by $\bar{\alpha}_0$ and interpreting $\hat{\mathbf{n}}_2$ as the antineutron direction in Eq. (1).

II. ANALYSIS

The analysis is based on $(1310.6 \pm 7.0) \times 10^6$ J/ψ events [28] collected with the BESIII detector, which is described in detail in Ref. [29]. The Λ hyperons are reconstructed using their $p\pi^-$ decays and the $\bar{\Lambda}$ hyperons using their $\bar{p}\pi^+$ or $\bar{n}\pi^0$ decays. The event reconstruction and selection procedure are described in Appendix A. The resulting data samples are essentially background free, as shown in Figs. A.1 and A.2. A Monte Carlo (MC) simulation including all known J/ψ decays is used to determine the background contribution. The sizes of the final data samples are 420,593 and 47,009 events with an estimated background of 399 ± 20 and 66.0 ± 8.2 events for the $p\pi^-\bar{p}\pi^+$ and $p\pi^-\bar{n}\pi^0$ final states, respectively. For each event the full set of the kinematic variables $\boldsymbol{\xi}$ is reconstructed.

The free parameters describing the angular distributions for the two data sets — α_ψ, $\Delta\Phi$, α_-, α_+, and $\bar{\alpha}_0$ — are determined from a simultaneous unbinned maximum likelihood fit. In the fit, the likelihood function is constructed from the probability density function $\mathcal{P}(\boldsymbol{\xi}^{(i)}) = \mathcal{C}(\alpha_\psi, \Delta\Phi, \alpha_-, \alpha_2) \times \mathcal{W}(\boldsymbol{\xi}^{(i)}; \alpha_\psi, \Delta\Phi, \alpha_-, \alpha_2)$ with $\alpha_2 = \alpha_+$ and $\alpha_2 = \bar{\alpha}_0$ for the $p\pi^-\bar{p}\pi^+$ and $p\pi^-\bar{n}\pi^0$ data sets, respectively. The final configuration of an event i is characterized by the vector $\boldsymbol{\xi}^{(i)}$, and $\mathcal{W}(\boldsymbol{\xi}^{(i)}; \alpha_\psi, \Delta\Phi, \alpha_-, \alpha_2)$ is given by Eq. (1). The normalization of the probability function, $\mathcal{C}(\alpha_\psi, \Delta\Phi, \alpha_-, \alpha_2)$, is determined for each parameter set using a sum of the weights $\mathcal{W}(\boldsymbol{\xi}^{(m)}; \alpha_\psi, \Delta\Phi, \alpha_-, \alpha_2)$ for an ensemble $\boldsymbol{\xi}^{(m)}$ of isotropically generated MC events (with $\mathcal{W}(\boldsymbol{\xi}; 0, 0, 0, 0) \equiv 1$). The generated events are propagated through a computer model of the BESIII detector and filtered using the same selection criteria as for the experimental data. The resulting global fit describes the multidimensional angular distributions very well as shown in Figs. A.3 and A.4. In a crosscheck the fit was applied to the two data sets separately and the obtained values of the parameters agree within statistical uncertainties as shown in Table A.1. The details of the fit as well the evaluation of the systematic uncertainties are discussed in Appendix A, and the contributions to the systematic uncertainty are listed in Table A.2.

TABLE I. Summary of the results: the $J/\psi \to \Lambda\bar{\Lambda}$ angular distribution parameter α_ψ, the phase $\Delta\Phi$, the asymmetry parameters for the $\Lambda \to p\pi^-$ (α_-), $\bar{\Lambda} \to \bar{p}\pi^+$ (α_+) and $\bar{\Lambda} \to \bar{n}\pi^0$ ($\bar{\alpha}_0$) decays, the CP asymmetry A_{CP}, and the ratio $\bar{\alpha}_0/\alpha_+$. The first uncertainty is statistical, and the second one is systematic.

Parameters	This work	Previous results
α_ψ	$0.461 \pm 0.006 \pm 0.007$	0.469 ± 0.027 [25]
$\Delta\Phi$	$(42.4 \pm 0.6 \pm 0.5)^\circ$	–
α_-	$0.750 \pm 0.009 \pm 0.004$	0.642 ± 0.013 [27]
α_+	$-0.758 \pm 0.010 \pm 0.007$	-0.71 ± 0.08 [27]
$\bar{\alpha}_0$	$-0.692 \pm 0.016 \pm 0.006$	–
A_{CP}	$-0.006 \pm 0.012 \pm 0.007$	0.006 ± 0.021 [27]
$\bar{\alpha}_0/\alpha_+$	$0.913 \pm 0.028 \pm 0.012$	–

III. RESULTS

A clear polarization, strongly dependent on the Λ direction, $\cos\theta_\Lambda$, is observed for Λ and $\bar{\Lambda}$. In Fig. 2, the moment $\mu(\cos\theta_\Lambda) = (1/N) \sum_i^{N(\theta_\Lambda)} (n_{1,y}^{(i)} - n_{2,y}^{(i)})$, related to the polarization, is calculated in 50 bins in $\cos\theta_\Lambda$. N is the total number of events in the data sample and $N(\theta_\Lambda)$ is the number of events in a $\cos\theta_\Lambda$ bin. In the limit of CP conservation, $\alpha_- = -\alpha_+$, while an approximate isospin symmetry leads to $\alpha_+ \approx \bar{\alpha}_0$ [16, 30], and the expected angular depen-

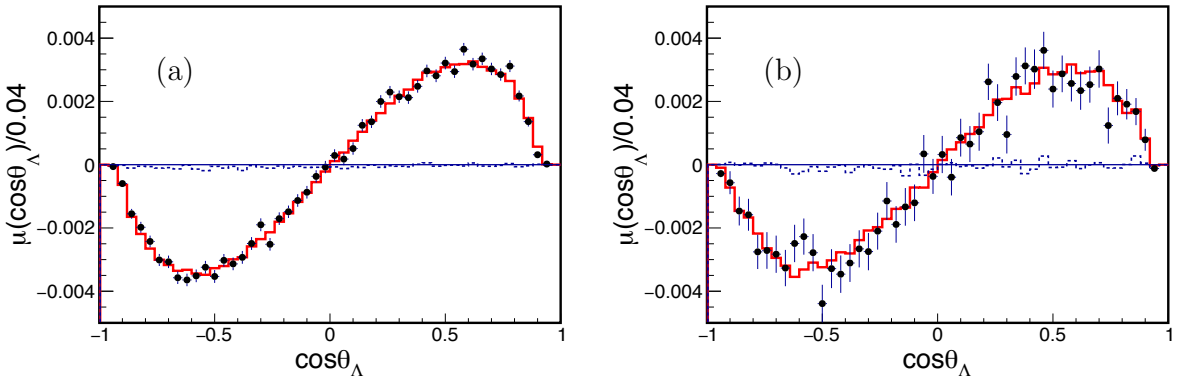

FIG. 2. Moments $\mu(\cos\theta_\Lambda)$ for acceptance uncorrected data as a function of $\cos\theta_\Lambda$ for (a) $p\pi^-\bar{p}\pi^+$ and (b) $p\pi^-\bar{n}\pi^0$ data sets. The points with error bars are the data, and the solid-line histogram is the global fit result. The dashed histogram shows the no polarization scenario ($\mathcal{W}(\boldsymbol{\xi};0,0,0,0)\equiv 1$).

dence is $\mu(\cos\theta_\Lambda) \sim \sqrt{1-\alpha_\psi^2}\alpha_-\sin\Delta\Phi\cos\theta_\Lambda\sin\theta_\Lambda$ for the acceptance corrected data (compare Eq. (1)). The phase between helicity flip and helicity conserving transitions is determined to be $\Delta\Phi = (42.4 \pm 0.6 \pm 0.5)^\circ$, where the first uncertainty is statistical and the second systematic. This large value of the phase enables a simultaneous determination of the decay asymmetry parameters for $\Lambda \to p\pi^-$, $\bar{\Lambda} \to \bar{p}\pi^+$, and $\bar{\Lambda} \to \bar{n}\pi^0$ as given in Table I. The value of $\alpha_- = 0.750 \pm 0.009 \pm 0.004$ differs by more than five standard deviations from the commonly accepted world average value of $\alpha_-^{\rm PDG} = 0.642 \pm 0.013$, based on elaborate experiments from 1963-75 [13–17], where the daughter proton polarization was measured in a secondary scattering process. Our result means that all published measurements on $\Lambda/\bar{\Lambda}$ polarization, determined from the product of α_- and the polarization, are $(17 \pm 3)\%$ too large. The obtained value for the ratio $\bar{\alpha}_0/\alpha_+$ is 3σ lower than unity, the value expected from the $|\Delta I| = \frac{1}{2}$ rule for non-leptonic decays of strange particles [16, 31], indicating the importance of radiative corrections [30, 32]. The α_- and α_+ values determined in this Letter, together with the covariance matrix, enable a calculation of the CP odd observable $A_{CP} = (\alpha_- + \alpha_+)/(\alpha_- - \alpha_+) = -0.006 \pm 0.012 \pm 0.007$. This is the most sensitive test of CP violation for the Λ baryon with a substantially improved precision over previous measurements [9] (Table I) and using a novel, model independent method. The Cabibbo-Kobayashi-Maskawa (CKM) mechanism predicts an A_{CP} value of $\sim 10^{-4}$ [33], while various extensions of the standard model predict larger value [34], in an attempt to explain the observed baryon-antibaryon asymmetry in the universe. This new method for CP tests, when applied to the foreseen future larger data samples, can reach a precision level compatible with theory predictions, which in turn will give a clue about baryogenesis.

ACKNOWLEDGMENTS

The BESIII collaboration thanks the staff of BEPCII and the IHEP computing center for their strong support. This work is supported in part by National Key Basic Research Program of China under Contract No. 2015CB856700; National Natural Science Foundation of China (NSFC) under Contracts Nos. 11335008, 11375205, 11425524, 11625523, 11635010, 11735014; the Chinese Academy of Sciences (CAS) Large-Scale Scientific Facility Program; the CAS Center for Excellence in Particle Physics (CCEPP); Joint Large-Scale Scientific Facility Funds of the NSFC and CAS under Contracts Nos. U1532257, U1532258, U1732102, U1732263; CAS Key Research Program of Frontier Sciences under Contracts Nos. QYZDJ-SSW-SLH003, QYZDJ-SSW-SLH040; 100 Talents Program of CAS; the CAS President's International Fellowship Initiative; INPAC and Shanghai Key Laboratory for Particle Physics and Cosmology; German Research Foundation DFG under Contracts Nos. Collaborative

Research Center CRC 1044, FOR 2359; Istituto Nazionale di Fisica Nucleare, Italy; Koninklijke Nederlandse Akademie van Wetenschappen (KNAW) under Contract No. 530-4CDP03; Ministry of Development of Turkey under Contract No. DPT2006K-120470; National Science and Technology fund; The Swedish Research Council; the Knut and Alice Wallenberg foundation; U. S. Department of Energy under Contracts Nos. DE-FG02-05ER41374, DE-SC-0010118, DE-SC-0010504, DE-SC-0012069; University of Groningen (RuG) and the Helmholtzzentrum fuer Schwerionenforschung GmbH (GSI), Darmstadt.

Appendix A: Methods

1. Monte Carlo simulation

The optimization of the event selection criteria and the estimation of backgrounds are based on Monte Carlo (MC) simulations. The GEANT4-based simulation software includes the geometry and the material description of the BESIII spectrometer, the detector response and the digitization models, as well as the data base of the running conditions and the detector performance. The production of the J/ψ resonance is simulated by the MC event generator KKMC[35]; the known decays are generated by BESEVTGEN[36, 37] with branching ratios set to the world average values [27], and missing decays are generated by the LUNDCHARM[38] model with optimized parameters[39]. Signal and background events are generated using helicity amplitudes. For the signal process, $J/\psi \to \Lambda\bar{\Lambda}$, the angular distribution of Eq. (1) is used. For the backgrounds, $J/\psi \to \Sigma^0\bar{\Sigma}^0$, $\Sigma^+\bar{\Sigma}^-$ and $\Lambda\bar{\Sigma}^0 + c.c$ decays, the helicity amplitudes are taken from Ref.[40], and the angular distribution parameters are fixed to -0.24 [41] for $J/\psi \to \Sigma^0\bar{\Sigma}^0$ and $J/\psi \to \Sigma^+\bar{\Sigma}^-$, and to 0.38 [42] for $J/\psi \to \Lambda\bar{\Sigma}^0 + c.c.$

2. Selection Criteria

Charged tracks detected in the Main Drift Chamber (MDC) must satisfy $|\cos\theta| < 0.93$, where θ is the polar angle with respect to the beam direction. There are no particle identification requirements for the tracks. Showers in the Electromagnetic Calorimeter (EMC), not associated with any charged track, are identified as photon candidates if they fulfill the following requirements: the deposited energy is required to be larger than 25 MeV and 50 MeV for clusters reconstructed in the barrel ($|\cos\theta| < 0.8$) and end cap ($0.86 < |\cos\theta| < 0.92$), respectively. In order to suppress electronic noise and showers unrelated to the event, the EMC time difference from the event start time is required to be within [0, 700] ns. To remove showers originating from charged particles, the angle between the shower position and charged tracks extrapolated to the EMC must be greater than 10 degrees.

a. Selection of $\boldsymbol{J/\psi \to \Lambda\bar{\Lambda},\ \Lambda \to p\pi^-,\ \bar{\Lambda} \to \bar{p}\pi^+}$ Events with at least four charged tracks are selected. Fits of the Λ and $\bar{\Lambda}$ vertices are performed using all pairs of positive and negative charged tracks. There should be at least one $\Lambda\bar{\Lambda}$ pair in an event. If more than one set of $\Lambda\bar{\Lambda}$ pairs is found, the one with the smallest value of $(M_{p\pi^-} - M_\Lambda)^2 + (M_{\bar{p}\pi^+} - M_\Lambda)^2$, where M_Λ is the nominal $\Lambda(\bar{\Lambda})$ mass, is retained for further analysis. A four constraint kinematic fit imposing energy-momentum conservation (4C-fit) is performed with the $\Lambda \to p\pi^-$ and $\bar{\Lambda} \to \bar{p}\pi^+$ hypothesis, and events with $\chi^2 < 60$ are retained. The invariant masses of $p\pi^-$ and $\bar{p}\pi^+$ are required to be within $|M_{p\pi^-} - M_\Lambda| < 5$ MeV/c^2 and $|M_{\bar{p}\pi^+} - M_\Lambda| < 5$ MeV/c^2. The $p\pi^-$ and $\bar{p}\pi^+$ invariant mass spectra and the selection windows are shown in Fig. A.1.

b. Selection of $\boldsymbol{J/\psi \to \Lambda\bar{\Lambda},\ \Lambda \to p\pi^-,\ \bar{\Lambda} \to \bar{n}\pi^0}$ Events with at least two charged tracks and at least three showers are selected. Two showers, consistent with being photons, are used to reconstruct the π^0 candidates, and the invariant mass of the pair is required to be in the interval $[0.12, 0.15]$ GeV/c^2. To improve the momentum resolution, a mass-constrained fit to the π^0 nominal mass is applied to the photon pairs, and the resulting energy and momentum of the π^0 are used for further analysis. Candidates for Λ are formed by combining two oppositely charged tracks into the final states $p\pi^-$. The two daughter tracks are constrained to originate from a common decay vertex by requiring the χ^2 of the vertex fit to be less than 100. To identify a $\bar{n}$ shower, the deposited energy in the EMC is required to be larger than 350 MeV, and the second moment of the cluster is required to be larger than 20. The moment is defined as $\sum_i E_i r_i^2 / \sum_i E_i$, where E_i is the deposited energy in the i-th crystal, and r_i is the radial distance of the crystal i from the cluster center. To select the $J/\psi \to \Lambda(p\pi^-)\bar{\Lambda}(\bar{n}\pi^0)$ candidate events, a one-constraint (1C) kinematic fit is performed, where

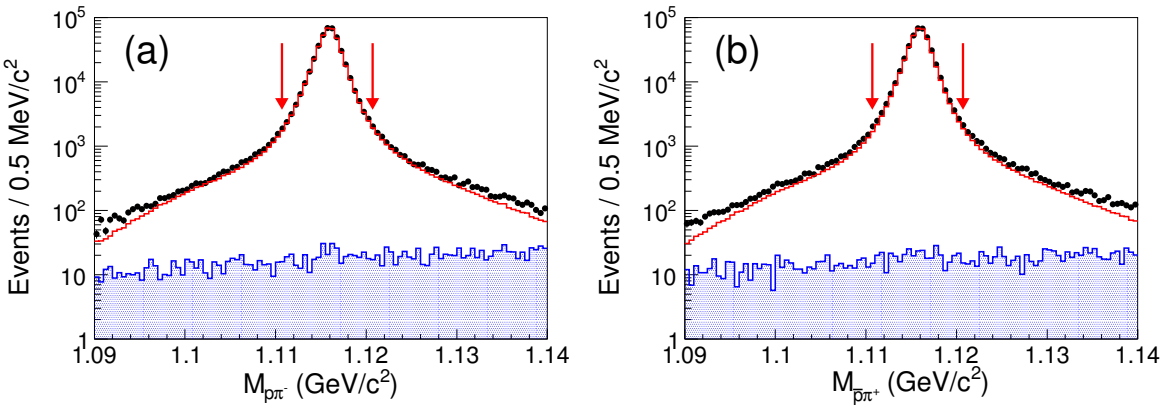

FIG. A.1. Distribution for (a) invariant mass of $p\pi^-$ and (b) invariant mass of $\bar{p}\pi^+$. The dots with error bars and the open histogram denote data and signal MC, respectively. The shaded histogram shows the background. The arrows indicate the Λ and $\bar{\Lambda}$ mass windows used to select the signal events.

the momentum of the anti-neutron is unmeasured. The selected events should have the $\chi^2_{1C-\bar{n}}$ of the 1C kinematic fit less than 10, and if there is more than one combination, the one with the smallest $\chi^2_{1C-\bar{n}}$ value is chosen. To further suppress background contributions, we require $|M_{p\pi^-} - M_\Lambda| < 5$ MeV/c^2, where M_Λ is the Λ nominal mass. Figure A.2 shows the invariant mass ($M_{\bar{n}\pi^0}$) of the $\bar{n}\pi^0$ pair and the mass $M^{\rm Recoiling}_{\Lambda\pi^0}$ recoiling against the $\Lambda\pi^0$, where $M_{\bar{n}\pi^0} = \sqrt{(E_{\bar{n}}+E_{\pi^0})^2-(\vec{P}_{\bar{n}}+\vec{P}_{\pi^0})^2}$, $\vec{P}_{\bar{n}} = -(\vec{P}_\Lambda+\vec{P}_{\pi^0})$ is in the rest frame of J/ψ, and $E_{\bar{n}} = \sqrt{|\vec{P}_{\bar{n}}|^2+M_n^2}$ (with M_n the nominal neutron mass). The signal regions are defined as $|M_{\bar{n}\pi^0} - M_\Lambda| < 23$ MeV/c^2 and $|M^{\rm Recoiling}_{\Lambda\pi^0} - M_n| < 7$ MeV/c^2 as shown in Fig. A.2.

c. Background analysis The potential backgrounds are studied using the inclusive MC sample for J/ψ decays. After applying the same selection criteria as for the signal, the main backgrounds for the $\bar{\Lambda}\to\bar{p}\pi^+$ final state are from $J/\psi\to\gamma\Lambda\bar{\Lambda}$, $\Lambda\bar{\Sigma}^0+c.c.$, $\Sigma^0\bar{\Sigma}^0$, $\Delta^{++}\bar{p}\pi^- + c.c.$, $\Delta^{++}\bar{\Delta}^{--}$, and $p\pi^-\bar{p}\pi^+$ decays. Decays of $J/\psi\to\Lambda\bar{\Sigma}^0+c.c.$ and $\Sigma^0\bar{\Sigma}^0$ are generated using the helicity amplitudes and include subsequent Λ and $\bar{\Lambda}$ decays. The remaining decay modes are generated according to the phase space model, and the contribution is shown in Fig. A.1. For the $\bar{\Lambda}\to\bar{n}\pi^0$ final state, the dominant background processes are from the decay modes $J/\psi\to\gamma\Lambda\bar{\Lambda}$, $\Lambda\bar{\Sigma}^0+c.c.$, $\Sigma^0(\gamma\Lambda)\bar{\Sigma}^0(\gamma\bar{\Lambda})$, $\Sigma^+(p\pi^0)\bar{\Sigma}^-(\bar{n}\pi^-)$, $\Lambda(p\pi^-)\bar{\Lambda}(\bar{p}\pi^+)$. Exclusive MC samples for these backgrounds are generated and used to estimate the background contamination shown in Fig. A.2.

3. The global fit

Based on the joint angular distribution shown in Eq. (1), a simultaneous fit is performed to the two data sets according to the decay modes:

$$\begin{aligned}&\text{I: } J/\psi\to\Lambda\bar{\Lambda},\ \Lambda\to p\pi^-\text{ and }\bar{\Lambda}\to\bar{p}\pi^+,\\ &\text{II: } J/\psi\to\Lambda\bar{\Lambda},\ \Lambda\to p\pi^-\text{ and }\bar{\Lambda}\to\bar{n}\pi^0.\end{aligned}$$

There are three common parameters, α_ψ, $\Delta\Phi$ and α_-, and two separate parameters α_+ and $\bar{\alpha}_0$ for the $\bar{\Lambda}$ decays to $\bar{p}\pi^+$ and $\bar{n}\pi^0$, respectively. For data set I, the joint likelihood function is defined as[40]:

$$\mathcal{L}^{\rm I} = \prod_{i=1}^{N^{\rm I}}\mathcal{P}(\xi_{\rm I}^{(i)}) = (\mathcal{C}^{\rm I})^{N^{\rm I}}\prod_{i=1}^{N^{\rm I}}\mathcal{W}(\xi_{\rm I}^{(i)};\alpha_\psi,\Delta\Phi,\alpha_-,\alpha_+), \tag{A1}$$

where $\mathcal{P}(\xi_{\rm I}^{(i)})$ is the probability density function evaluated for event i, and $\mathcal{W}(\xi_{\rm I}^{(i)};\alpha_\psi,\Delta\Phi,\alpha_-,\alpha_+)$ is calculated with Eq. (1) for event i. The normalization factor, $(\mathcal{C}^{\rm I})^{-1} = \frac{1}{N_{\rm MC}}\sum_{j=1}^{N_{\rm MC}}\mathcal{W}(\xi_{\rm I}^{(j)};\alpha_\psi,\Delta\Phi,\alpha_-,\alpha_+)$, is estimated with the accepted $N_{\rm MC}$ events, which are generated with the phase space model, undergo detector simulation, and are selected with the same event criteria as for data. The definition of the likelihood function for data set II, $\mathcal{L}^{\rm II}$, is the same

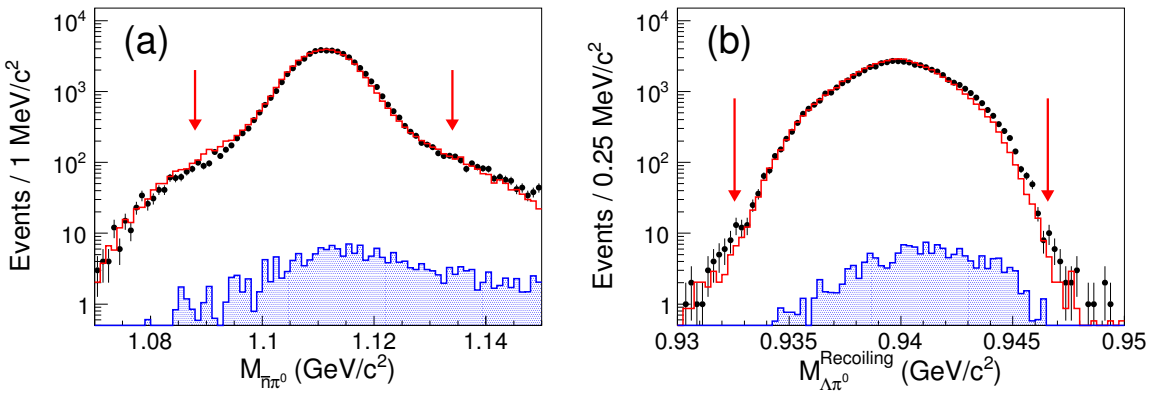

FIG. A.2. Distribution for (a) invariant mass of $\bar{n}\pi^0$ and (b) recoiling mass of $\Lambda\pi^0$. The dots with error bars and the open histograms denote data and signal MC, respectively. The shaded histograms show the backgrounds. The arrows indicate the selection windows.

except for its calculation with different parameters and data set. To determine the parameters, we use the package MINUIT from the CERN library [43] to minimize the function defined as:

$$S = -\ln\mathcal{L}^{\rm I}_{\rm data} - \ln\mathcal{L}^{\rm II}_{\rm data} + \ln\mathcal{L}^{\rm I}_{\rm bg.} + \ln\mathcal{L}^{\rm II}_{\rm bg.}, \quad \text{(A2)}$$

where $\ln\mathcal{L}^{\rm I(II)}_{\rm data}$ and $\ln\mathcal{L}^{\rm I(II)}_{\rm bg.}$ are the likelihood functions for the two data sets and the background events, respectively. The results of the separate fits for the two data sets are given in Table A.1. We compare the fit with the data using moments T_i $(i = 1, ..., 5)$ directly related to the terms in Eq. (1). The moments are explicitly given by

$$T_1 = \sum_i^{N(\theta_\Lambda)} \left(\sin^2\theta_\Lambda n^{(i)}_{1,x} n^{(i)}_{2,x} + \cos^2\theta_\Lambda n^{(i)}_{1,z} n^{(i)}_{2,z}\right),$$

$$T_2 = -\sum_i^{N(\theta_\Lambda)} \sin\theta_\Lambda\cos\theta_\Lambda (n^{(i)}_{1,x} n^{(i)}_{2,z} + n^{(i)}_{1,z} n^{(i)}_{2,x}),$$

$$T_3 = -\sum_i^{N(\theta_\Lambda)} \sin\theta_\Lambda\cos\theta_\Lambda n^{(i)}_{1,y},$$

$$T_4 = -\sum_i^{N(\theta_\Lambda)} \sin\theta_\Lambda\cos\theta_\Lambda n^{(i)}_{2,y},$$

$$T_5 = \sum_i^{N(\theta_\Lambda)} \left(n^{(i)}_{1,z} n^{(i)}_{2,z} - \sin^2\theta_\Lambda n^{(i)}_{1,y} n^{(i)}_{2,y}\right).$$

Figs. A.3 and A.4 show the fit results to data sets I and II, respectively. The distributions of T_i $(i = 1, ..., 5)$ functions in terms of $\cos\theta_\Lambda$, and the Λ angular distribution are shown in histograms (a)-(f), together with the corresponding pull distributions. The asymmetric distributions of T_3 and T_4 indicate that significant transverse polarization of Λ and $\bar{\Lambda}$ hyperons is observed. The simultaneous fit results for α_ψ, α_-, α_+, $\Delta\Phi$ and $\bar{\alpha}_0$ parameters are given in Table A.1. Based on these parameters, the observables $\bar{\alpha}_0/\alpha_+$ and $A_{CP} = (\alpha_- + \alpha_+)/(\alpha_- - \alpha_+)$ are calculated, and their statistical uncertainties are evaluated taking into account correlation coefficients $\rho(\alpha_+, \alpha_0) = 0.42$ and $\rho(\alpha_+, \alpha_-) = 0.82$, respectively. As a cross check, separate fits to data sets I and II are performed, and results are consistent with the simultaneous fit within statistical uncertainties, as given in Table A.1.

TABLE A.1. Simultaneous fit results for the angular distribution parameter, α_ψ, $\Delta\Phi$ and the asymmetry parameters α_- for decays $\Lambda \to p\pi^-$, α_+ for $\bar{\Lambda} \to \bar{p}\pi^+$ and α_0 for $\bar{\Lambda} \to \bar{n}\pi^0$, and compared to the separate fit results to data I and II samples. The uncertainties are statistical only.

Pars.	Simultaneous fit	Fit to I	Fit to II
α_ψ	0.461 ± 0.006	0.459 ± 0.006	0.473 ± 0.019
α_-	0.750 ± 0.009	0.749 ± 0.010	0.756 ± 0.031
α_+	-0.758 ± 0.010	-0.759 ± 0.010	.....
$\bar{\alpha}_0$	-0.692 ± 0.016	.....	-0.684 ± 0.028
$\Delta\Phi$ (°)	42.4 ± 0.6	42.3 ± 0.6	43.4 ± 2.1

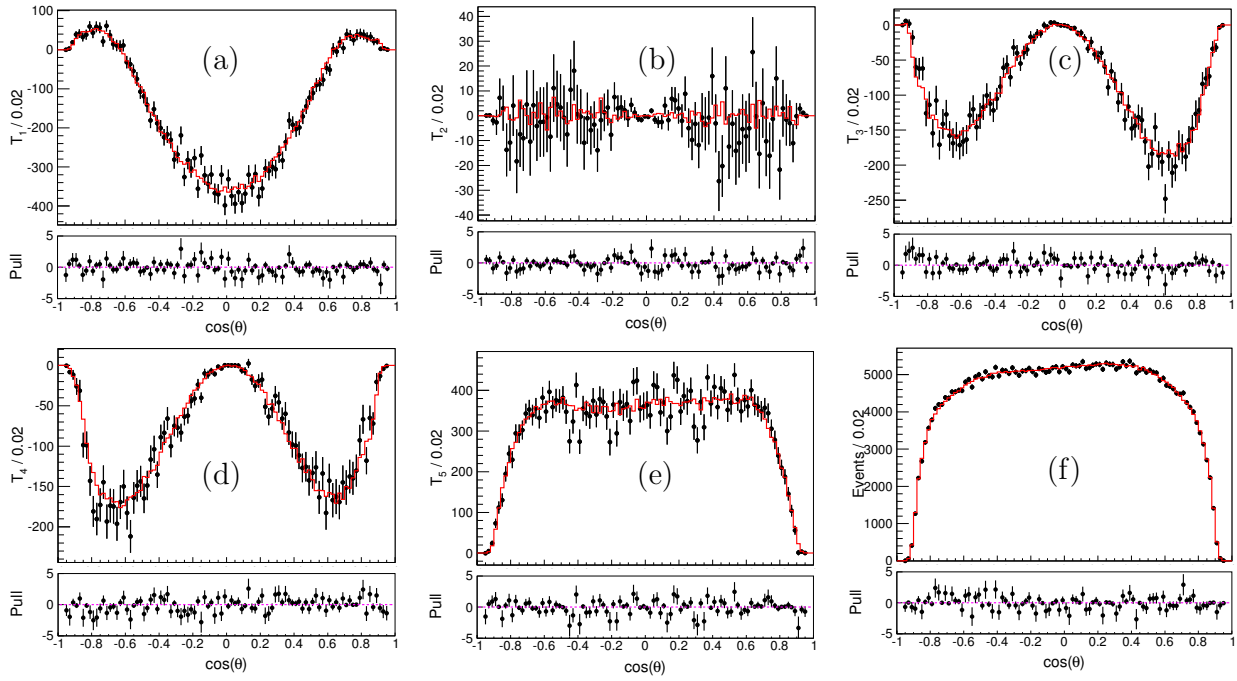

FIG. A.3. Distributions of T_i $(i = 1, ..., 5)$ functions in terms of $\cos\theta_\Lambda$, and the Λ angular distribution for the decays $J/\psi \to \Lambda\bar{\Lambda}$, $\Lambda \to p\pi^-$ and $\bar{\Lambda} \to \bar{p}\pi^+$. The dots with error bars are the data, and the histograms are the total fit results. The pull distribution is shown at the bottom of each histogram.

4. Systematic uncertainty

The systematic uncertainties can be divided into two categories. The first category is from the event selection, including the uncertainties on MDC tracking efficiency, the kinematic fit, π^0 and $\bar{n}$ efficiencies, Λ and $\bar{\Lambda}$ reconstruction, background estimations, and the Λ, $\bar{\Lambda}$ and $M^{\rm Recoiling}_{\Lambda\pi^0}$ mass window requirements. The second category includes uncertainties associated with the fit procedure.

1. The uncertainty due to the efficiency of the charged particles tracking has been investigated with $J/\psi \to \Lambda\bar{\Lambda} \to p\pi^-\bar{p}\pi^+$ control samples[44], taking into consideration the correlation between the magnitude of charged particle momentum and its polar angle acceptances. Corrections are made based on the 2-dimensional distribution of momentum versus polar angle. The difference between the fit results with and without the tracking correction is taken as a systematic uncertainty.

2. The uncertainty due to the π^0 reconstruction is estimated from the difference between data and MC simulation using a $J/\psi \to \pi^+\pi^-\pi^0$ control sample. The uncertainty due to $\bar{n}$ shower requirement is estimated with a $J/\psi \to p\pi^-\bar{n}$ control sample, and the correction factors between data and MC simulations are determined. The differences in the fit results with and without corrections to the efficiencies of the π^0 and $\bar{n}$ reconstructions are taken as systematic uncertainties.

3. The systematic uncertainties for the determination of the physics parameters in the fits due to the Λ and $\bar{\Lambda}$ vertex reconstructions are found to be negligible.

4. The systematic uncertainties due to kinematic fits are determined by making corrections to the track parameters in the MC simulations to better match the data. The corrections are done with the 5-dimensional distributions over the θ_Λ, $\hat{\mathbf{n}}_1$, $\hat{\mathbf{n}}_2$ variables, where the $\hat{\mathbf{n}}_1$ and $\hat{\mathbf{n}}_2$ are

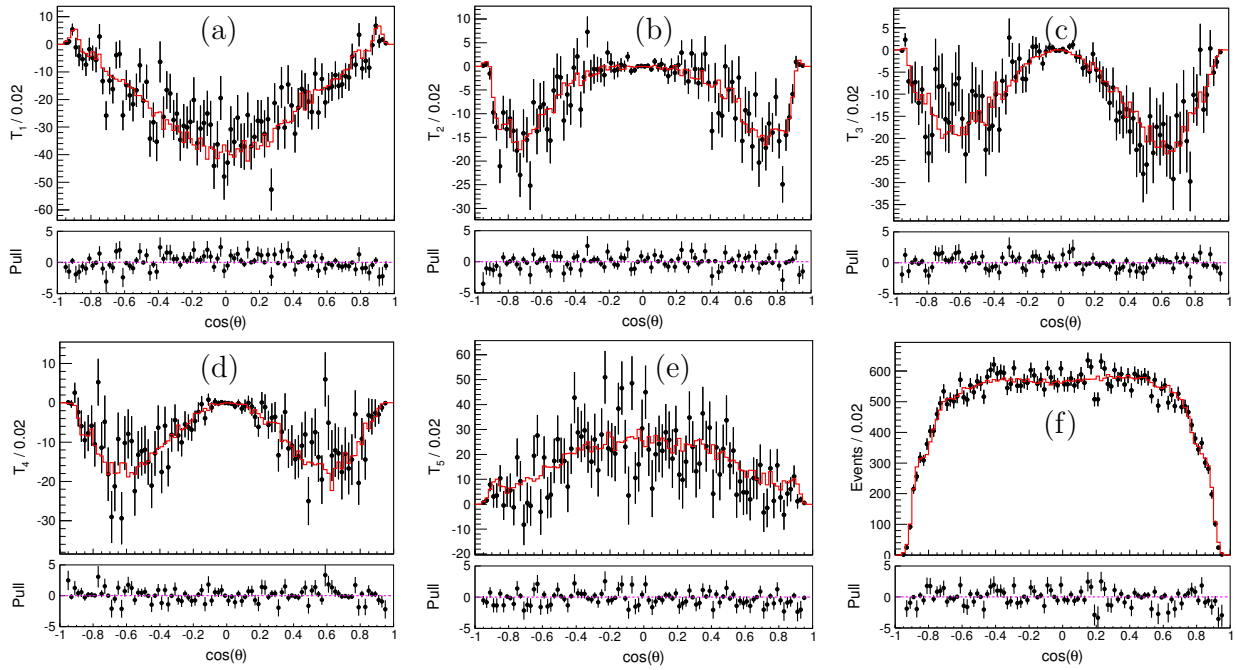

FIG. A.4. Distributions of T_i $(i = 1, ..., 5)$ functions in terms of $\cos\theta_\Lambda$, and the Λ angular distribution for decays $J/\psi \to \Lambda\bar{\Lambda}$, $\Lambda \to p\pi^-$ and $\bar{\Lambda} \to \bar{n}\pi^0$. The dots with error bars are the data, and the histograms are the total fit results. The pull distribution is shown at the bottom of each plot.

expressed using spherical coordinates. The fit to data with the corrected MC sample yields α_ψ=0.462 $\pm$ 0.006, $\alpha_- = 0.749 \pm 0.009$, $\alpha_+ = -0.752 \pm 0.009$, and $\bar{\alpha}_0 = -0.688 \pm 0.017$. The differences between the fit with corrections and the nominal fit are considered as the systematic uncertainties. For α_ψ, the difference between the fit results with and without this correction is negligible.

5. The uncertainty due to the fit method is estimated with MC simulations. The differences between the input and output values on the physical parameters are taken as the systematic uncertainties.

6. The systematic uncertainty caused by the background estimation is studied by fitting the data with and without considering background subtraction. The differences on the parameters are taken as the systematic uncertainties. The contamination rate of background events in this analysis is less than 0.1% according to the full MC simulations, and the uncertainty due to background estimation is negligible.

TABLE A.2. Relative systematic uncertainties (%) for the measurements of parameters $\alpha_{J/\psi}$, α_-, α_+, $\bar{\alpha}_0$ and $\Delta\Phi$. Uncertainties due to the $\Lambda/\bar{\Lambda}$ vertex and backgrounds are ignored.

Source	$\alpha_{J/\psi}$	α_-	α_+	$\bar{\alpha}_0$	$\Delta\Phi$
Tracking,π^0, $\bar{n}$	1.5	0.1	0.3	0.6	1.1
Kinematic fit	0.2	0.1	0.8	0.6	0.0
Fit method	0.0	0.5	0.4	0.4	0.1
Total	1.5	0.5	0.9	0.8	1.1

The total systematic uncertainty for the parameters is obtained by summing the individual systematic uncertainties in quadrature, and is summarized in Table A.2.

[1] L. Kopke and N. Wermes, Phys. Rept. **174**, 67 (1989).
[2] N. Cabibbo and R. Gatto, Phys. Rev. **124**, 1577 (1961).
[3] S. J. Brodsky, C. E. Carlson, J. R. Hiller, and D. S. Hwang, Phys. Rev. **D69**, 054022 (2004).
[4] G. Fäldt and A. Kupsc, Phys. Lett. **B772**, 16 (2017).
[5] G. Bunce *et al.*, Phys. Rev. Lett. **36**, 1113 (1976).
[6] L. G. Pondrom, Phys. Rept. **122**, 57 (1985).
[7] B. E. Bonner *et al.*, Phys. Rev. **D38**, 729 (1988).
[8] K. B. Luk *et al.*, Phys. Rev. **D38**, 19 (1988).
[9] P. D. Barnes *et al.*, Phys. Rev. **C54**, 1877 (1996).
[10] A. Chakravorty *et al.* (FNAL E756), Phys. Rev. Lett. **91**, 031601 (2003).
[11] G. Aad *et al.* (ATLAS), Phys. Rev. **D91**, 032004 (2015).
[12] L. Adamczyk *et al.* (STAR), Nature **548**, 62 (2017).
[13] J. W. Cronin and O. E. Overseth, Phys. Rev. **129**, 1795 (1963).
[14] O. E. Overseth and R. F. Roth, Phys. Rev. Lett. **19**, 391 (1967).
[15] P. M. Dauber, J. P. Berge, J. R. Hubbard, D. W. Merrill, and R. A. Muller, Phys. Rev. **179**, 1262 (1969).
[16] W. E. Cleland, G. Conforto, G. H. Eaton, H. J. Gerber, M. Reinharz, A. Gautschi, E. Heer, C. Revillard, and G. Von Dardel, Nucl. Phys. **B40**, 221 (1972).
[17] P. Astbury *et al.*, Nucl. Phys. **B99**, 30 (1975).
[18] A. Z. Dubnickova, S. Dubnicka, and M. P. Rekalo, Nuovo Cim. **A109**, 241 (1996).
[19] G. I. Gakh and E. Tomasi-Gustafsson, Nucl. Phys. **A771**, 169 (2006).
[20] H. Czyz, A. Grzelinska, and J. H. Kuhn, Phys. Rev. **D75**, 074026 (2007).
[21] G. Fäldt, Eur. Phys. J. **A51**, 74 (2015).
[22] G. Fäldt, Eur. Phys. J. **A52**, 141 (2016).
[23] J. Z. Bai *et al.* (BES), Phys. Lett. **B424**, 213 (1998), [Erratum: Phys. Lett.B438,447(1998)].
[24] M. Ablikim *et al.* (BESII), Chin. Phys. **C36**, 1031 (2012).
[25] M. Ablikim *et al.* (BESIII), Phys. Rev. **D95**, 052003 (2017).
[26] T. D. Lee and C.-N. Yang, Phys. Rev. **108**, 1645 (1957).
[27] C. Patrignani *et al.* (Particle Data Group), Chin. Phys. **C40**, 100001 (2016).
[28] M. Ablikim *et al.* (BESIII), Chin. Phys. **C41**, 013001 (2017).
[29] M. Ablikim *et al.* (BESIII), Nucl. Instrum. Meth. **A614**, 345 (2010).
[30] S. Olsen, L. Pondrom, R. Handler, P. Limon, J. A. Smith, and O. E. Overseth, Phys. Rev. Lett. **24**, 843 (1970).
[31] F. S. Crawford, J. M. Cresti, R. L. Douglass, M. L. Good, and H. K. Ticho, Phys. Rev. Lett. **2**, 266 (1959).
[32] A. A. Belavin and I. M. Narodetsky, Yad. Fiz. **8**, 978 (1968).
[33] J. F. Donoghue, X.-G. He, and S. Pakvasa, Phys. Rev. **D34**, 833 (1986).
[34] I. I. Bigi, X.-W. Kang, and H.-B. Li, Chin. Phys. **C42**, 013101 (2018).
[35] S. Jadach, B. F. L. Ward, and Z. Was, Comput. Phys. Commun. **130**, 260 (2000).
[36] D. J. Lange, *Proceedings, 7th International Conference on B physics at hadron machines (BEAUTY 2000): Maagan, Israel, September 13-18, 2000*, Nucl. Instrum. Meth. **A462**, 152 (2001).
[37] R.-G. Ping, Chin. Phys. **C32**, 599 (2008).
[38] J. C. Chen, G. S. Huang, X. R. Qi, D. H. Zhang, and Y. S. Zhu, Phys. Rev. **D62**, 034003 (2000).
[39] R.-L. Yang, R.-G. Ping, and H. Chen, Chin. Phys. Lett. **31**, 061301 (2014).
[40] B. Zhong, R.-G. Ping, and Z.-J. Xiao, Chin. Phys. **C32**, 692 (2008).
[41] M. Ablikim *et al.* (BES), Phys. Lett. **B632**, 181 (2006).
[42] M. Ablikim *et al.* (BESIII), Phys. Rev. **D86**, 032008 (2012).
[43] F. James and M. Roos, Comput. Phys. Commun. **10**, 343 (1975).
[44] M. Ablikim *et al.* (BESIII), Phys. Rev. **D89**, 052001 (2014).